International Journal of Technology and Engineering System (IJTES)
Vol 7. No.3 2015 Pp. 230-238

available at : www.ijcns.com
ISSN: 0976-1345

CLASSIFICATION OF TYPES OF GLAUCOMA BASED ON ANTERIOR CHAMBER REGION ASSESSMENT OF HD-OCT IMAGES

PROFESSOR S. J. GRACE SHOBA, M. KUMARESH, R. SIVASHANKAR, I. NAVEEN

ABSTRACT

Glaucoma is an ocular disease that results in permanent blindness. Improper filtration of the intra-ocular fluid inside the human eye increases the intra-ocular pressure and alters the position of retinal layers especially iris and cornea resulting in Glaucoma. Glaucoma is classified as Open Angle Glaucoma (OAG) and Angle Closure Glaucoma (ACG) based on the irido-corneal parameters. The treatment methods incorporated for OAG and ACG are different from each other. Thus, early detection of Glaucoma and its classification is very essential. In this project, an algorithm is proposed to automatically extract the retinal feature values and to detect the presence of Glaucoma and classify the disease. High Definition Optical Coherence Tomography (HD-OCT) serves as a fast, accurate and non-invasive modality for the anterior segment of the eye. The input OCT images are pre-processed by applying binary filtering to conceal the irrelevant intensity distribution, segmented by Otsu's thresholding to characterize the texture of changes, morphologically filtered to smooth the segmented region. The feature values such as the Angle between iris and cornea, Area, Equivalent Diameter, Perimeter, and Aspect Ratio of the anterior chamber are then computed. The Probabilistic neural network classifier is trained with the extracted feature values to accurately classify the type of Glaucoma. The proposed algorithm proved to be more efficient and effective by providing a classification accuracy rate of 93.33% in less than 2 seconds

***Index Terms*—Anterior chamber, bilateral filtering, classifier, morphological filtering, Otsu thresholding, retinal features.**

INTRODUCTION

GLAUCOMA is the second leading cause of irreversible visual loss next to cataract, according to [1], data from World Health Organization. It is characterized by the progressive loss of axons in the optic nerve. Glaucoma is more common in Asians and an immediate detection tool is essential

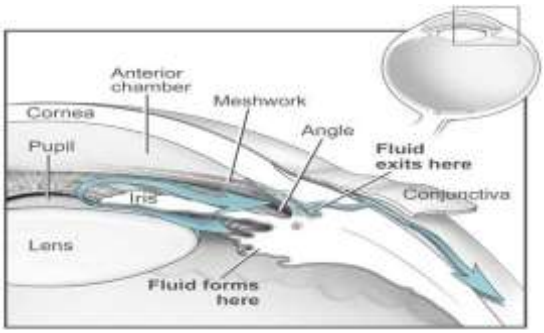

to characterize the disease existence and classify the same. Glaucoma is generally of two types based on the feature values between the iris and cornea.

1) Open Angle glaucoma, the most common form of glaucoma, accounting for at least 90% of all glaucoma cases is caused by the slow clogging of the drainage canals, resulting in increased eye pressure. It has a wide and open angle between the iris and cornea. It develops slowly and is a lifelong condition and has symptoms and damage that are not noticed. Open Angle Glaucoma means that the angle where the iris meets the cornea is as wide and open as it should be. Open-angle glaucoma is also called primary or chronic glaucoma. It is the most common type of glaucoma, affecting about three million Asians, Americans.

2) Angle Closure Glaucoma, a less common form of glaucoma is caused by blocked drainage canals, resulting in a sudden rise in intraocular pressure and has a closed or narrow angle between the iris and cornea. It develops very quickly and has symptoms and damage that are usually very noticeable. It demands immediate medical attention.

It is also called acute glaucoma or narrow-angle glaucoma. Unlike Open Angle Glaucoma, Angle Closure Glaucoma is a result of the angle between the iris and cornea closing. It is estimated that ACG, which is mainly found in Asians (87%), will cause 5.5 million people bilateral blindness by2020 [2]. Hence, screening and diagnosis of ACG is more important, especially in Asia. Given that glaucoma is asymptomatic in the early stage and is often only recognized when the disease is quite

advanced and vision is lost, the detection of ACG using Asia. Given that glaucoma is asymptomatic in the early stage and is often only recognized when the disease is quite advanced and vision is lost, the detection of ACG using clinical imaging modalities could aid in arresting its development or slow down the progression.

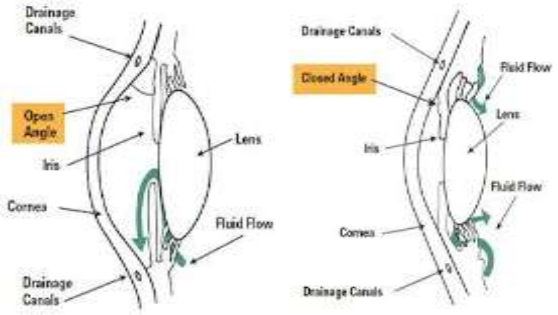

Fig. 2. Anterior chamber of the human eye visualizing glaucomatous eyes with open angle and angle closure between the iris and cornea.

Hence Anterior Chamber assessment plays a vital role in Glaucoma assessment. Though many modern techniques and instruments are available to assess the anterior chamber angle, those techniques stand invasive, costlier and are not available to the common population. Assessment of the retinal fundus images to compute the optic cup to optic disc ratio also serves as tool for glaucoma detection. But this technique does not sound effective and stands inaccurate and inefficient. Also, the results obtained are not accurate to the point and time consuming. The most common two approaches, namely, gonioscopy and Ultrasound Bio-Microscopy (UBM) are generally used for visualizing and measuring the anterior chamber angle in specific.

A. Gonioscopy

Gonioscopy is considered as the general reference standard for the evaluation of the anterior chamber angle. Gonioscopy was introduced by Trantas in 1899 [3]. Though gonioscopy is considered as the "gold standard," it is highly subjective in measurement purposes. The angle findings vary across various grading schemes, and there is no universal standard for measurement. It is more prone to measurement errors due to the positioning of the lens on the eye [4] and different illumination intensities.

B. Ultrasound Bio-Microscopy (UBM)

Ultrasound Bio-microscopy is considered as an alternative approach for viewing anterior chamber angle. It uses higher frequency transducer than the regular ultrasound for more detailed assessment of the anterior ocular structures [5]. A semi automated program was designed in this technique to compute the important parameters based on the manual identification of the scleral spur, which is more prone to intraobserver and interobserver.

II . HD – OPTICAL COHERENCE TOMOGRAPHY

During the past decade we have witnessed tremendous development in visualization techniques for the posterior segment of the eye and anterior segment of the eye using techniques like gonioscopy and Ultra Bio-Microscopy. Time domain Optical Coherence Tomography (TD-OCT) impressed the retina specialists but was soon left in the shade by Spectral domain OCT (SD-OCT), which offered higher resolution range of 1 μm to 3 μm axial resolution with SD-OCT versus 10 μm with TD-OCT and 3-D imaging possibilities. Swept Source OCT (SS-OCT) is the latest milestone in retinal and choroidal imaging. To overcome scattering by the Retinal Pigment Epithelium (RPE), which disabled visualization of deeper lying structures, a longer wavelength was adopted for this machine (1050 nm versus 840 nm in SD-OCT), and photo detectors instead of CCD cameras led to a further increase in resolution (1 μm).

The scan speed in swept source instruments is twice that of SD-OCT devices (100000 A-scans/sec compared with 50000 A-scans/sec), enabling faster acquisition of B-scans, thus allowing us to obtain wide field B-scans (12 mm versus 6–9 mm with conventional SD-OCT) and more accurate 3-D imaging of the vitreous, retina, and choroid. Wide scans make it possible to present the optic nerve and macula on the same scan. Simultaneous high-quality visualization of the vitreous, retina, and choroid is possible. Choroidal layers that are hardly distinguishable in conventional SD-OCT become visible. The new SS-OCT confirms earlier histologic data: the structure of the choroid consists of multiple layers going from the innermost Bruch membrane to the choriocapillaris, Sattler layer (layer of medium diameter blood vessels), Haller layer (outermost layer of the choroid consisting of larger diameter blood vessels), and lamina suprachoroidea.

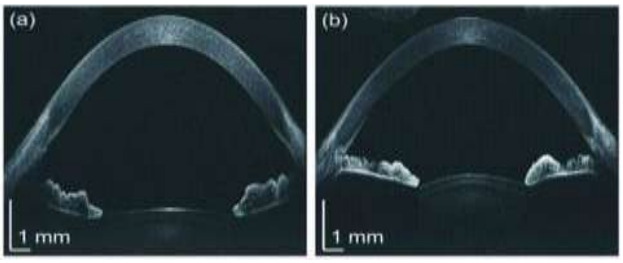

Fig. 3. High Definition Swept Source Optical Coherence Tomography (SS-OCT) images showing the (a) glaucomatous eye of a patient with open angle and (b) glaucomatous eye of a patient with angle closure.

Thus SS-OCT images are used as input to process the anterior segment of eye to detect and classify the glaucoma.

III . PROPOSED SYSTEM DESIGN

The architecture of the overall proposed system is shown in Fig. 4. It mainly consists of five steps, pre-processing, segmentation of anterior chamber, post-processing, anterior segment shape analysis – feature extraction and glaucoma type classification using neural networks. The explanation of the system design follows the architecture of the proposed system.

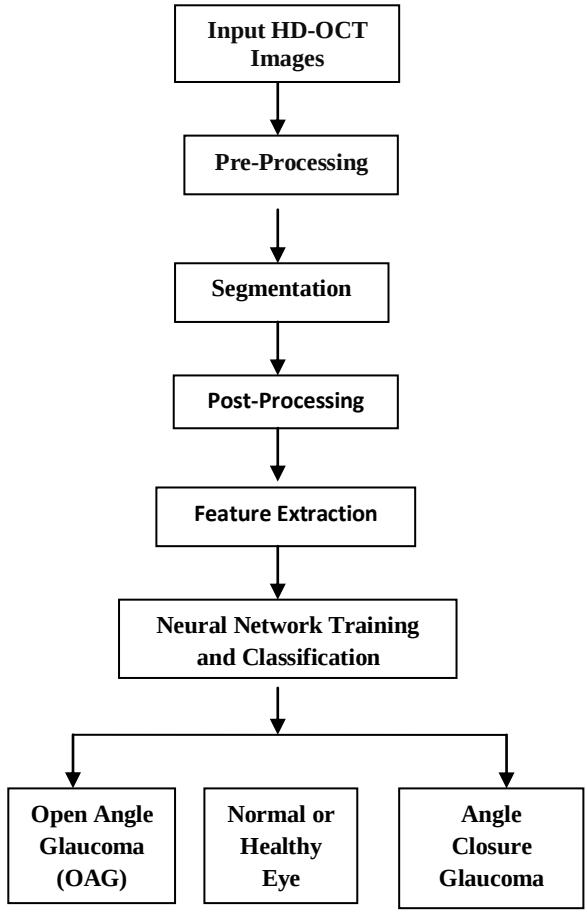

Fig.4. Architecture and flow chart representation of the proposed system design showing various blocks.

Let us now discuss the processing of each block in detail as follows.

A. Input HD-OCT Images

The input High Definition, Swept Source Optical Coherence Tomography database of images was collected from an Ophthalmic Hospital.

Fig. 5. High Definition Swept Source Optical Coherence Tomography (SS-OCT) images showing Open Angle Glaucoma, Normal or Healthy eye, Angle Closure Glaucoma respectively, that are used as input images to the system.

Around 45 images were collected which included 15 images with Open Angle Glaucoma, 15 images with Angle Closure Glaucoma and 15 images belonging to normal or healthy eye.

B. Pre-Processing

In the pre-processing module, the noisy input image will be enhanced by reducing the noises such as speckle or Gaussian noise using bilateral filtering. A bilateral filter is a non-linear, edge-preserving and noise reducing smoothing filter for images. The intensity value at each pixel in an image is replaced by a weighted average of intensity values from nearby pixels. This weight can be based on a Gaussian distribution. The weights depend not only on Euclidean distance of pixels, but also on the radiometric differences (e.g. range differences, such as color intensity, depth distance, etc.). This preserves sharp edges by systematically looping through each pixel and adjusting weights to the adjacent pixels accordingly. The bilateral filter is defined as,

$$I^{\text{filtered}}(x) = \frac{1}{W_p} \sum_{x_i \in \Omega} I(x_i) f_r(\|I(x_i) - I(x)\|) g_s(\|x_i - x\|),$$

Where the normalization function is given,

$$W_p = \sum_{x_i \in \Omega} f_r(\|I(x_i) - I(x)\|) g_s(\|x_i - x\|)$$

Where,

- Ifiltered (x) is the filtered image.
- I is the original input image to be filtered.
- x are the co-ordinates of the current pixel.
- Ω is the window centered in x.
- fr is the range kernel for smoothing differences in intensities. This may be a Gaussian function.
- gs is the spatial kernel for smoothing differences in coordinates. This function can be a Gaussian function.

The input noisy image and the bilaterally filtered, denoised image are comparatively shown below in Fig. 6.

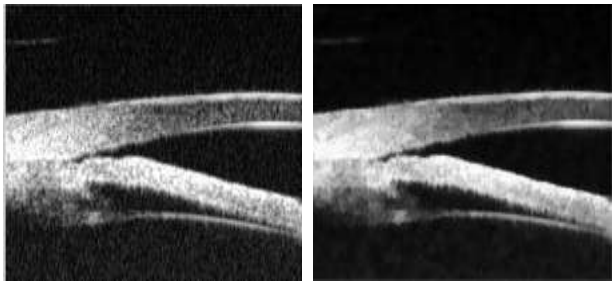

Fig. 6. The first figure represents the input noisy input and the second figure represents the image denoised using a bilateral filter – pre-processing.

B . Segmentation

Image segmentation is the process of partitioning an image into non-intersecting regions such that each region is homogeneous. Here Otsu thresholding method is used. It is used to measure the average foreground and background variance to suppress the redundant region to zero's and set one's to desired foreground. It is used to obtain an optimal threshold that maximizes a function of the threshold level. In Otsu's method we exhaustively search for the threshold that minimizes the intra-class variance (the variance within the class), defined as a weighted sum of variances of the two classes:

$$\sigma_w^2(t) = \omega_1(t)\sigma_1^2(t) + \omega_2(t)\sigma_2^2(t)$$

Weights w_i are the probabilities of the two classes separated by a threshold t and variances of these classes. Otsu shows that minimizing the intra-class variance is the same as maximizing inter-class variance:

$$\sigma_b^2(t) = \sigma^2 - \sigma_w^2(t) = \omega_1(t)\omega_2(t)\left[\mu_1(t) - \mu_2(t)\right]^2$$

This is expressed in terms of class probabilities and class means. The class probability is given by,

$$\omega_1(t) = \Sigma_0^t p(i)$$

The class mean is given by,

$$\mu_1(t) = \left[\Sigma_0^t p(i)\, x(i)\right] / \omega_1$$

The algorithm flow for the segmentation process is discussed in Fig. 7.

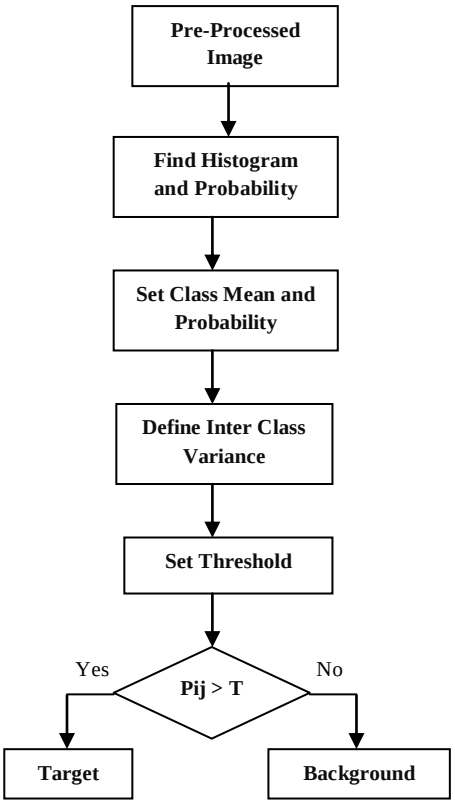

Fig. 7. Algorithm used for Segmentation – Otsu thresholding

Fig. 8. Segmented binary image obtained by implemented Otsu thresholding algorithm on the pre-processed image.

This probability based image segmentation is helpful to extract the region feature from the labelled single band image.

D. Post-Processing

Post-Processing includes morphological filtering functions like dilation and erosion. Morphological operations are applied on segmented binary image for smoothening the foreground region. It processes the image based on shapes and it performs on image using structuring element. The structuring elements will be created with specified shapes (disk, line, square) which contains 1's and 0's value where ones represents the neighbourhood pixels. Dilation and erosion process is used to enhance the object region by removing the unwanted pixels from outside region of foreground object. The output pixel is determined by using these processing

pixel neighbours. Here, the 'disk' structuring element is used to dilate and erode the image for smoothing. Dilation is the process of adding a pixel at object boundary based on structuring element. The rule to find output pixel is the maximum of input pixels neighbourhood matrix. Erosion is to remove the pixel from the object boundary depends on structuring element. The rule to find output pixel is the maximum of input pixels neighbourhood matrix. The output image is smoothened by reducing distortion from background and edge sharpness. The below figure shows the algorithm used for morphological operations.

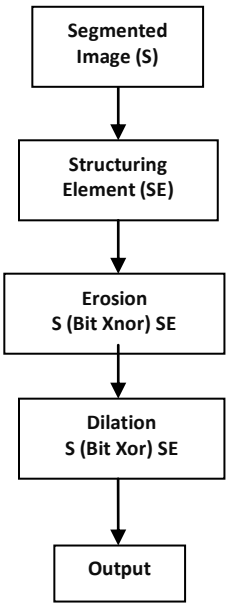

Fig. 9. Flowchart showing Morphological operations performed on segmented image.

The erosion of *A* by *B* is given by the expression.

$$A \ominus B = \bigcap_{b \in B} A_{-b}$$

The dilation of *A* by the structuring element *B* is defined by

$$A \oplus B = \bigcup_{b \in B} A_b$$

The below Fig. 10. Represents the post processed image.

Fig. 10. Post-Processed Image showing the foreground and background.

E. Feature Extraction

After post-processing, the pixels are applied for connected component analysis and then for the analysis of the object region for counting the objects. Connected component analysis is a process to label the segmented image foreground pixels with 4 or 8 neighbourhood connectivity. It is used to separate the image into n number of local objects from grouping of similar pixels. Then the irrelevant background objects with maximum area arre removed using the morphological process to obtain desired objects. Finally the anterior chamber region will be filtered out from segmented image for extraction of features related to shape.

The angle between the iris and cornea is computed using the Pythagoras theorem. The other feature values such as the area, perimeter, equivalent diameter and aspect ratio (ratio of the width to height of the anterior segment) of the anterior segment of the eye are computed using mat lab coding commands. The anterior chamber region will now be utilized to extract geometrical features to discriminate the different category images. The chamber will be described by measuring the following characteristics, angle, equivalent diameter, perimeter, area, aspect ratio. The below figure depicts the area in which the feature values are computed.

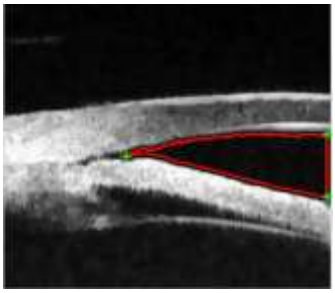

Fig. 11. Demarcation of anterior chamber region of the human eye that is used to extract the feature values.

The Pythagoras theorem used to measure the angle between the iris and cornea is explained below with the mathematical formulations and figures.

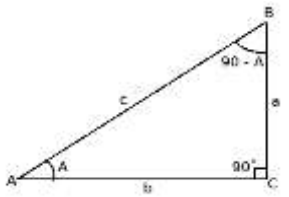

Fig. 12. Pythagorean Theorem identity used to compute the angle From the triangle ABC, the trigonometric identities can be written as,

Sin A = a / c

Cos A = b / c

Tan A = Sin A / Cos A

Tan A = a / b

Where "a" is the height and "b" is the width of the anterior chamber. The obtained feature values are then used to train the neural network classifier for automatic classification of the input images. The below table represents the features values obtained to train the classifier for classifying the input images.

TABLE I
FEATURE VALUES TO TRAIN THE CLASSIFIER

Features	CAG	Normal Eye	OAG
Angle (degrees)	<20	20–30	>30
Perimeter (mm)	100-490	490-600	>600
Diameter (mm)	10-80	90-120	120-600
Aspect Ratio	2-4	1-3	1-2
Area (mm^2)	500-5000	5000-8000	8000-11200

F. Neural Network Training and Classification

In the proposed system, supervised learning with non knowledge based classifier called probabilistic neural network is used for image classification. The neural network model PNN is used here to act as a classifier with radial basis function for network activation function. The training sample features with assigned target vectors are fed into created PNN model for supervised training to get network parameters such as node biases and weighting factors. Finally, test image features are simulated with trained network to make decision of OCT image such as normal or glaucomatous.

The network classifies the input vector into a specific class because that particular class has the maximum probability to be correct. The PNN has three layers: the Input Layer, Radial Basis Layer and the Competitive layer. Radial Basis Layer evaluates vector distances between input vector and row weight vectors in weight matrix. These distances are scaled by Radial Basis Function nonlinearly. Competitive Layer finds the shortest distance among them, and thus finds the training pattern closest to the input pattern based on their distance. The vector distances between input vector p and the weight vector made of each row of weight matrix **W** are calculated. Here, the vector distance is defined as the dot product between two vectors. The architecture of the PNN classifier is discussed below. Assume the dimension of W is Q×R. The dot product between p and the ith row of W produces the ith element of the distance vector ||W-p||, whose dimension is Q×1. The minus symbol, "-", indicates that it is the distance between vectors. Then, the bias vector b is combined with ||W- p|| by an element-by-element multiplication. The result is denoted as n = ||W- p||.*b. The transfer function in PNN has built into a distance criterion with respect to a center. This layer is defined as radbas (n) = e-n^2. Each element of n is substituted and it produces corresponding element of a, the output vector of Radial Basis Layer.

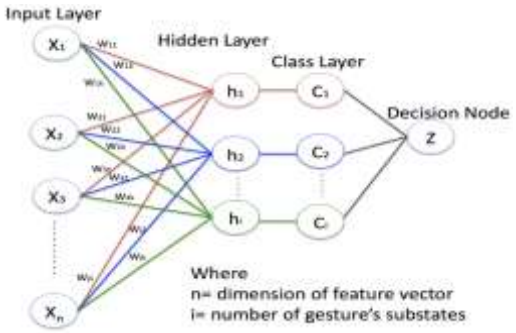

Fig. 13. Architecture of Probabilistic Neural Network Classifier

The ith element of a can be represented as the ai = radbas (||Wi - p||.*b) where Wi is the vector made of the ith row of W and p. A radial basis neuron with a weight vector close to the input vector p produces a value near 1 and then its output weights in the competitive layer will pass their values to the competitive function. It is also possible that several elements of a are close to 1 since the input pattern is close to several training patterns.

The pnn is trained with reference features set and desired output using 'newpnn' command. Here, target 1 is set for normal, 2 and 3 for each abnormal case as desired output. After the training, updated weighting factor and biasing with other network parameters are stored to simulate with input features. At the classification stage, test image features are utilized to simulate with trained network model using 'sim' command. Finally it returns the classified value which is one of either 1, 2, or 3. Based on that the decision will be taken whether the give input image is normal or with OAG OR CAG.

IV. EXPERIMENTS AND DISCUSSIONS

The processing time and the performance specifications of our proposed system are evaluated in the following sections.

A. Processing Time

The algorithm is implemented in MATLAB R2009a using an Intel Core 2 Duo CPU P7450 _a 2.13 GHz and 1.72 GHz computer. The average processing time of each stage is computed and listed as follows:

1) Pre-Processing: 0.317 s;
2) Segmentation: 0.35 s;
3) Post-Processing: 0.20 s;
4) Feature Extraction: 0.514 s;
5) Classification: 0.436 s;
6) Total: 1.817 s.

Hence, the proposed system can computer the features of the anterior segment thereby classify the type of glaucoma present in an individual in less than two seconds which is less time consuming for the ophthalmologists.

B. PERFORMANCE SPECIFICATIONS

The performance of the proposed system can be evaluated through the following parameters.

1) Accuracy
2) Sensitivity
3) Specificity

Sensitivity measures the proportion of actual positives which are correctly identified. It is given by the relation,

Sensitivity = TP / (TP + FN)

Where, TP = True Positive – Abnormal image correctly classified as Abnormal, FN = False Negative - Abnormality incorrectly classified as normal. Specificity measures the proportion of negatives which are correctly identified. It is given by,

Specificity = TN / (FP + TN)

Where, FP = False Positive - Normal image incorrectly classified as Abnormal, TN = True negative, Normal image correctly classified as normal. The total accuracy of the system is given using the relation,

Total accuracy = (TN+TN) / (TP+TN+FN+FN)

The system provides an overall accuracy rate of 100%. The system computes the feature values for all the input images accurately and can provide a classification accuracy rate of 100% for all the input images.

V. CONCLUSION AND FUTURE WORK

Glaucoma is a major blinding disease that causes irreversible blindness. In this proposed system, we introduced a novel method to detect the presence of Glaucoma and classify the same using DIP. We processed the input image and extracted five important features of the anterior chamber namely area, equivalent diameter, perimeter, angle, aspect ratio. Based on the obtained feature values the classifier has been trained to classify the Glaucoma type so as to initiate appropriate treatment to the patients. As a future work, we would like to introduce some more parameters for classifying the disease and deal with the sub-type classification of glaucoma for more precise and accurate results.

ACKNOWLEDGMENT

The authors thank the technicians at the Ophthalmic Hospital, Chennai, for gathering the dataset of images and for informative discussions. Professor S. J. Grace Shoba is currently working at Velammal Engineering College, Chennai. She is a lifetime member of ISTE and IETE. She is pursuing PhD in the field of Image Processing and has a teaching experience of over 15 years in various reputed institutions. She has over 6 publications to her credit and has presented papers in various national and international conferences. M. Kumaresh was born in Chennai in 1994. He is currently pursuing his Bachelors in Engineering in Electronics and Communication Engineering in Velammal Engineering College, Chennai. He has presented many research papers and research projects in the field of wireless communication and embedded systems in many national level technical symposiums and conferences in top notch universities across India. His areas of interests include medical electronics and communication systems. He is a life time member of IETE and IEEE.

R. Sivashankar was born in Sirkali in 1993. He is currently pursuing his Bachelors in Engineering in Electronics and Communication Engineering in Velammal Engineering College, Chennai. He has presented many research papers and research projects in the field of medical electronics and signal processing in many national level technical symposiums and conferences in top notch universities across India. His areas of interest include modern electronics and signal processing. He is a life time member of IETE and IEEE.

I. Naveen was born in Dharmapuri in 1994. He is currently pursuing his Bachelors in Engineering in Electronics and Communication Engineering in Velammal Engineering College, Chennai. He is interested in digital electronics and microprocessor systems. He is doing research works in his area of interest. He has presented papers and projects in top universities across India.

REFERENCES

[1] A. Giangiacomo and A. L. Coleman, The Epidemiology of Glaucoma. Berlin Heidelberg, Germany: Springer-Verlag, 2009, ch. 2, pp. 13–21.

[2] A. T. Broman and H. A. Quigley, "The number of people with glaucoma worldwide in 2010 and 2020," Br. J. Ophthalmol., vol. 90, pp. 262–267, 2006.

[3] A. Dellaport, "Historical notes on gonioscopy," Surv. Ophthalmol., vol. 20, pp. 137–149, 1975.

[4] D. S. Friedman and H. Mingguang, "Anterior chamber angle assessment techniques," Surv. Ophthalmol., vol. 53, no. 3, pp. 250–273, 2007.

[5] C. Pavlin, M. Sherar, and F. FS, "Subsurface ultrasound microscopic imaging of the intact eye," Ophthalmology, vol. 97, no. 2, pp. 244–250, Feb. 1990.

[6] H. Ishikawa, K. Esaki, L. JM, Y. Uji, and R. Ritch, "Ultrasound Biomicroscopy dark room provocative testing: A quantitative method for estimating anterior chamber angle width," Jpn. J. Ophthalmol., vol. 43, no. 6, pp. 526–534, Nov./Dec. 1999.

[7] W. P. Nolan, J. L. See, P. T. Chew, D. S. Friedman, S. D. Smith, S. Radhakrishnan, C. Zheng, P. J. Foster, and T. Aung, "Detection of primary angle closure using anterior segment optical coherence tomography in asian

eyes," Ophthalmology, vol. 114, no. 1, pp. 33–39, Jan. 2007.
[8] J. W. Console, L. M. Sakata, T. Aung, D. S. F. Man, and M. He, "Quantitative analysis of anterior segment optical coherence tomography images: The Zhongshan angle assessment program," Br. J. Ophthalmol., vol. 92, pp. 1612–1616, 2008.
[9] The certainty of Cirrus. Carl Zeiss Meditec. [Online]. Available: http://www.cirrusoctdemo.com/index.html
[10] Visante omni: A new dimension in anterior segment evaluation, Carl Zeiss Meditec, Inc., Zeiss, 2007.
[11] Cirrus HD-OCTUserManual Addendum-Anterior Segment Imaging, Carl Zeiss Meditec, Inc., Zeiss, 2007.
[12] H.-T. Wong, M. C. Lim, L. M. Sakata, H. T. Aung, N. Amerasinghe, D. S. Friedman, and T.Aung, "High-definition optical coherence tomography imaging of the iridocorneal angle of the eye," Arch.Ophthalmol., vol. 127, no. 3, pp. 256–260, 2009.
[13] C.Y. Cheung, C. Zheng, C.-L. Ho, T. A. Tun, R. S. Kumar, F. E. Sayyad, T. Y. Wong, and T. Aung, "Novel anterior-chamber angle measurements by high-definition optical coherence tomography using the schwalbe line as the landmark," Br. J. Ophthalmol., 2010. DOI: 10.1136/bjo.2010.189217.
[14] T. Jing, P. Marziliano, and H.-T.Wong, "Automatic detection of schwalbe's line in the anterior chamber of the eye using HD-OCT images," in Proc. 32nd Annu. Int. Conf. IEEE Eng. Biol. Soc., 2010.
[15] P. Soille, Morphological Image Analysis; Principles and Applications. Emeryville, CA: Springer-Verlag Telos, 2003.
[16] H. Samet and M. Tamminen, "Efficient component labeling of images of arbitrary dimension represented by linear bintrees," IEEE Trans. Pattern Anal. Mach. Intell., vol. 10, pp. 579–586, 1988.
[17] V. Westphal, A. M. Rollins, and S. Radhakrishnan, "Correction of Geometric and refractive image distortions in optical coherence Tomography applying fermat˙as principle," Opt. Express, vol. 10, no. 9, pp. 397–404, 2002.
[18] L. S. Lerner, Physics for Scientists and Engineers. Sudbury, MA: Jone and Bartlett Publishers, 1996.
[19] P. Y. Kim, K. M. Iftekharuddin, P. G. Davey, M. Tth, A. Garas, G. Holl and E. A. Essock,. Novel Fractal Feature-Based Multiclass Glaucoma Detection and Progression Prediction,. IEEE Journal of Biomedical and Health Informatics, vol. 17, no. 2, pp. 269-276, 2013.
[20] N. Otsu, .A threshold selection method from gray-level histograms,. IEEE Trans. Systems Man Cybernet vol. 9, pp. 62-66, 1979.